

Interaction of an outflow with surrounding gaseous clouds as the origin of the late-time radio flares in TDEs

JIALUN ZHUANG (庄嘉伦)^{1,2}, RONG-FENG SHEN (申荣锋)^{1,2}, GUOBIN MOU (牟国斌)³ AND WENBIN LU (鲁文宾)⁴

¹*School of Physics and Astronomy, Sun Yat-Sen University, Zhuhai, 519000, China*

²*CSST Science Center for the Guangdong-Hongkong-Macau Greater Bay Area, Sun Yat-Sen University, Zhuhai, 519082, China*

³*Department of Physics and Institute of Theoretical Physics, Nanjing Normal University, Nanjing 210023, China*

⁴*Department of Astronomy, University of California, Berkeley, CA 94720-3411, USA*

ABSTRACT

Close encounter between a star and a supermassive black hole (SMBH) results in the tidal disruption of the star, known as a tidal disruption event (TDE). Recently, a few TDEs, e.g., ASASSN-15oi and AT2018hyz, have shown late-time (hundreds of days after their UV/optical peaks) radio flares with radio luminosities of $10^{38\sim 39}$ erg/s. The super-Eddington fallback or accretion in a TDE may generate a mass outflow. Here we investigate a scenario that the late-time radio flares come from the interaction of the outflow with the circum-nuclear gaseous clouds, in addition to the slow-evolving emission component due to the outflow-diffuse medium interaction. We calculate the associated radio temporal and spectral signatures and find that they reproduce well the observations. The outflows have the inferred velocity of $0.2c \sim 0.6c$, the total mass of $10^{-3} \sim 10^{-1} M_{\odot}$ and the ejection duration of a month to a year. The distances of the clouds to the SMBH are $0.1 \sim 1$ pc. This scenario has advantages in explaining the long delay, sharpness of the rise and the multiplicity of the late radio flares. Future observations may build up a much larger sample of late-time radio flares and enable their use as a probe of the TDE physics and the host circumnuclear environment.

Keywords: Tidal disruption event, late-time radio flares

1. INTRODUCTION

Most galaxies are considered to contain a supermassive black hole (BH) with a mass above $\sim 10^6 M_{\odot}$ at its nuclei (Ferrarese & Ford 2005). A star wandering too close to the supermassive BH would be tidally disrupted as a tidal disruption event (TDE) (Rees 1988; Phinney 1989). Accretion of the stellar debris would produce a bright flare in X-ray or UV/optical, which would last for months to years with the light curve decaying as $t^{-\frac{5}{3}}$ (Rees 1988; Phinney 1989).

In TDEs, outflow can be produced via various mechanisms. At the moment of disruption, the unbound debris would fly away at a velocity of 10^4 km/s (Guillochon et al. 2016; Yalinewich et al. 2019). Besides, a fraction of the matter initially bound to the BH is likely to be blown away with a velocity of $\sim 0.1c$, where c is the light

speed, by the radiation pressure when the fallback rate, or the accretion rate, of these bound debris is super-Eddington at early times (Strubbe & Quataert 2009; Bu et al. 2023b). Furthermore, for BHs with masses greater than $10^7 M_{\odot}$, the self-crossing of the fallback stream, due to relativistic apsidal precession, can also generate energetic, fast outflow, and the speed of these outflow ranges from $\sim 0.01c$ to $\sim 0.1c$ (Lu & Bonnerot 2020). Another possibility concerns a relativistic jet which can be generated in the presence of a large magnetic flux threading a rapidly spinning BH (Blandford & Znajek 1977; Tchekhovskoy et al. 2011; Bloom et al. 2011; Burrows et al. 2011).

When the high-speed outflow or jet interacts with the circumnuclear medium (CNM), it would drive a forward shock in the CNM, and produce radio emission via the synchrotron radiation (Chevalier 1998; Barniol Duran et al. 2013). In the past decade, dozens of TDEs indeed have shown these GRB-afterglow-like radio emissions, and their radio luminosities span from 10^{36} to 10^{42} erg/s (Alexander et al. 2020).

E-mail: zhuangjlun@mail2.sysu.edu.cn (JZ);
shenrf3@mail.sysu.edu.cn (RS); gbmou@njnu.edu.cn (GM);
wenbinlu@berkeley.edu (WL)

However, recent TDEs radio observations reveal flares only seen at late times ($10^{2\sim 3}$ days after TDE discovery). Due to their steep rise of light curves, two typical cases being ASASSN-15oi (Horesh et al. 2021) and AT2018hyz (Cendes et al. 2022), they are difficult to be explained by the conventional outflow-CNM scenario. The steepest evolution from the outflow-CNM interaction is $f_\nu \propto t^3$ (Metzger et al. 2012; Krolik et al. 2016; Alexander et al. 2020), but ASASSN-15oi and AT2018hyz, show a jump in flux density from non-detection to detection that requires a temporal power-law steeper than t^4 . Similar ones were observed in IGR J12580+0134 (Perlman et al. 2022), AT2019azh (Sfaradi et al. 2022; Goodwin et al. 2022) and AT2020vwl Goodwin et al. (2023a,b, 2024).

Various models have been proposed to explain these late and steeply rising radio flares in TDEs. Cendes et al. (2023) conclude that the delayed outflows, such as from delayed disk formation, are a preferred explanation. However, early X-ray detection indicates that the accretion disk is already present early on (Guolo et al. 2023). So the outflow is expected to be launched at an early time without a time delay. Likewise, early radio detection such as AT2019azh suggests that the outflow tends to be launched at the occurrence of TDEs.

Teboul & Metzger (2023) propose a misaligned precessing jet, which is initially choked by the disk wind but later breaks out, when the disk eventually aligns itself with the BH spin axis. This jet may produce delayed radio rebrightening seen in TDEs. An alternative model is that of a decelerated off-axis jet (Matsumoto & Piran 2023; Sfaradi et al. 2024), which we will address in Section 5.

Besides, Matsumoto & Piran (2024) find that a CNM density profile that initially drops with radius in a power law but is followed by a constant outside the Bondi radius can explain the radio flares in AT2020vwl, AT2019dsg, PS16dtm and ASASSN14ae. However, this model is difficult to explain a rise steeper than $\propto t^3$, like those in AT2018hyz and ASASSN-15oi, unless the external density profile rises again. Lei et al. (2024) studied the collision of the unbound half of the stellar debris stream with an outer dusty torus. They show that it may produce a delayed (\sim years) radio flare with a rapid rise.

If discrete gaseous clouds exist in the circum-nuclear surroundings (see below), the TDE outflow will sweep across them. Mou et al. (2022) studied the outflow-cloud interaction and show that it can generate considerable radio emission months or years later after the TDE, and can explain the temporal evolution of the peak frequencies in AT2019dsg, ASASSN-14li, and CSS161010. Based on numerical simulations of the disk

wind launching, Bu et al. (2023a) further studied this model. Besides the delayed radio flare, the outflow-cloud interaction may have multi-messenger signatures including neutrinos, gamma-ray and X-ray (Mou & Wang 2021; Mou et al. 2021; Wu et al. 2022; Chen & Wang 2023).

Here, we investigate the outflow-cloud interaction model for these late-time radio flares. This collision forms a bow shock in front of the inner face of the cloud, across which electrons are accelerated and the magnetic field is amplified. The late-time radio synchrotron emission is expected from the shocked outflow. An illustration of the interaction of the TDE outflow with the cloud is shown in Figure 1.

In section 2, we introduce the semi-analytical model for the wind-cloud interaction and calculate the associated synchrotron emission. We take the effect of the interaction of the outflow with a diffuse CNM into account in section 3. The application of our model to a few TDEs is presented in section 4. Discussion and conclusion are given in sections 5 and 6, respectively.

2. THE OUTFLOW-CLOUD INTERACTION

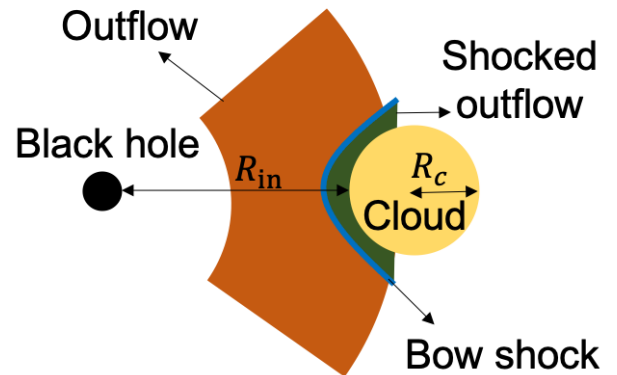


Figure 1. Schematic of the interaction of the TDE outflow with the cloud. Outflow is generated at the occurrence of TDEs with a half opening angle θ_w and a velocity v_w . The cloud is located at a distance of R_{in} with a radius R_c . The interaction of the outflow with the cloud leads to the formation of a bow shock, producing a late-time radio flare years after TDE. This illustration is not to scale.

2.1. The clouds

Observation of the Milky Way galactic center reveals tens of clouds near the Sgr A^* , and the distribution of these clouds indicates a ring-like structure (Mezger et al. 1996; Christopher et al. 2005). These clouds are at a distance of $0.5 \sim 2$ pc with a gas number density of

$10^6 \sim 10^8 \text{ cm}^{-3}$, and a mass of $10^{4\sim5} M_\odot$ (an estimated radius of $\sim 0.1 \text{ pc}$) (Mezger et al. 1996; Christopher et al. 2005).

As for AGN, the clouds have a size of $10^{13\sim14}$ with a higher density of $10^{8\sim9} \text{ cm}^{-3}$ (an estimated mass of $\sim 10^{-8} M_\odot$) at a similar distance of $10^{16\sim17} \text{ cm}$ (Armijos-Abendaño et al. 2022). Here we consider the simplest case where the outflow interacts with a cloud at a distance $R_{in} \approx 0.1 \sim 1 \text{ pc}$ and of a radius $R_c \approx 0.01 \sim 0.1 \text{ pc}$.

2.2. The outflow

After the disruption, the stellar debris will fall back to the vicinity of the BH after a so-called fall back timescale $t_{fb} = 130 R_{*,0}^{3/2} M_{*,0}^{-1} M_{bh,7}^{1/2} [\text{day}]$ (Guillochon & Ramirez-Ruiz 2013), and then form an accretion disk in a so-called circularization process which lasts for $\sim t_{fb}$ or longer. The outflow is launched when the BH is in the super-Eddington accretion phase. Meanwhile, the X-ray emission from the inner accretion flow is reprocessed by the outflow into optical emission, giving rise to the TDE's optical flare (e.g., Dai et al. 2018). Here we set the launching time of the accretion-driven outflow to be $t = 0$.

According to the simulation of the super-Eddington accretion in TDEs, the outflow is nearly spherical but largely anisotropic (Dai et al. 2018; Bu et al. 2023b). Its property depends sensitively on the inclination angle, i.e., it is faster and more dilute at a lower inclination angle (face-on with respect to the disk plane).

Nevertheless, the solid angle of the cloud is so small (~ 0.1) that the angular parts of the outflow that interact with it can be safely assumed to be isotropic. Besides, our primary aim is to demonstrate the potential of our model, i.e., to check whether this model can explain the observations with reasonable parameter values. So we do not take this inclination angle effect into account and consider the simplest case instead. We take the outflow to be conical and isotropic, with a half opening angle of $\theta_w = \pi/4$ (a solid angle of $\Omega_w \sim 2$) (Curd & Narayan 2019). The launching duration of the outflow is $t_w \sim$ months.

The outflow is set to have a mean velocity of v_w , and the velocities of its front and rear ends are $v_w \pm av_w$, respectively. Then its radial width grows as $\Delta(r) \approx 2ar + \Delta_0$, where $\Delta_0 = v_w t_w$ and $r = v_w t$. Numerical simulations of accretion-driven outflows suggest a radial velocity spread of $a \approx 0.1 \sim 0.6$ on particular inclination angles (see Figure 3 in Dai et al. 2018, or Figure 6 in Bu et al. 2023b). Hereafter we set $a=0.1$. The effect of a larger a will be discussed at the end of Section 2.4.

We define $\dot{m}(t', r)$ as the outflow's density at the elapsed time $t' = t - R_{in}/v_w$ at distance r . It is assumed to firstly increase linearly, then peak at $t_w(r) \equiv t_w \Delta(r)/\Delta_0$, and then decay in a power law of index $-\frac{5}{3}$:

$$\dot{m}_w(t', r) = \frac{\dot{m}_0 \Delta_0}{\Delta(r)} \times \begin{cases} \frac{t'}{t_w(r)}, & t' < t_w(r), \\ \left[\frac{t'}{t_w(r)} \right]^{-5/3}, & t_w(r) \leq t', \end{cases} \quad (1)$$

where \dot{m}_0 is the peak mass loss rate. The total mass of the outflow is $m_w = \int \dot{m}_w(t', r) dt'$.

2.3. Radiation properties

Assuming a fraction ϵ_b of the pre-shock outflow kinetic energy is converted into the magnetic energy density $B^2/(8\pi) = \epsilon_b \rho_w v_w^2$ (Sari et al. 1998; Yalinewich et al. 2019), the magnetic field strength is:

$$B = \sqrt{8\pi \epsilon_b \rho_w v_w} \\ \approx 0.1 \Omega_w^{-\frac{1}{2}} \epsilon_{b,-3}^{\frac{1}{2}} \dot{m}_{w,-1}^{\frac{1}{2}}(t', r) \beta_{w,-1}^{\frac{1}{2}} R_{in,-1}^{-1} [\text{G}] \quad (2)$$

where $\epsilon_{b,-3} \equiv \epsilon_b/0.001$, $\dot{m}_{w,-1}(t', r) \equiv \dot{m}_w(t', r)/(0.1 M_\odot/\text{yr})$, and $R_{in,-1} \equiv R_{in}/0.1 \text{ pc}$. Here ϵ_b has a wide range from 10^{-4} to 10^{-1} (Granot & van der Horst 2014; Santana et al. 2014; Zhang et al. 2015; Beniamini et al. 2016).

The peak synchrotron specific radiating power (per unit frequency) from an electron with a Lorentz factor of γ_e can be estimated as $P_{\nu,max} = P(\gamma_e)/\nu(\gamma_e) = m_e c^2 \sigma_t B / (3q_e)$ and is independent of γ_e (Sari et al. 1998). Thus, the peak specific flux of the swept-up electrons is $F_{\nu,max} = N_e P_{\nu,max} / (4\pi D^2)$, where D is the distance of the source and N_e is the total number of emitting electrons.

2.3.1. Time dependence of Radiating electrons

The number of emitting electrons at any given time t' is:

$$N_e(t') = \frac{\Omega_c \int_0^{t'} \dot{m}_w(t, r) dt}{\Omega_w m_p}, \quad (3)$$

where Ω_c is the cloud's solid angle and $\Omega_c/\Omega_w < 1$ is the fraction of the outflow that indeed interacts with the cloud.

However, these electrons would cool due to both radiation and expansion (e.g., Dai et al. 1999). The synchrotron cooling time for electrons with γ_e is (Sari et al. 1998)

$$t_{syn} = \frac{6\pi m_e c}{\sigma_t \gamma_e B^2} \\ = 7.7 \times 10^{10} \gamma_e^{-1} B_{-1}^{-2} [\text{s}]. \quad (4)$$

The adiabatic cooling timescale t_{ad} is generally estimated as the time required for the flow to cross the characteristic spatial scale $t_{dyn} \equiv R_c/v_w \approx 10^7 R_{c,-2} \beta_{w,-1}$ s where $R_{c,-2} \equiv R_c/0.01$ pc (Barkov et al. 2019). However, the simulation of the outflow-cloud interaction by Mou & Wang (2021) suggests that in the case of a long-lasting outflow $t_w \gg t_{dyn}$, the post-shock outflow stream is confined rather than expanding freely, while it approaches the free expansion if $t_w \leq t_{dyn}$. Therefore, we use the following fitting formula from Mou & Wang (2021, their Figure B2) to estimate

$$t_{ad} = \begin{cases} t_{dyn}, & (t_w/t_{dyn}) \leq 1, \\ 1.36t_w - 0.36t_{dyn}, & 1 < (t_w/t_{dyn}) < 15, \\ 20t_{dyn}, & 15 \leq (t_w/t_{dyn}). \end{cases} \quad (5)$$

The Lorentz factor of electrons which radiate mainly in GHz is about $\gamma_e \sim 50$ for $B \sim 0.1$ G. Then we have $t_{syn} \approx 10^9$ s $\gg t_{ad}$. Thus, the electron cooling is dominated by the adiabatic expansion.

Taking this cooling timescale into account, Eq. (3) would be corrected as:

$$N_e(t') = \frac{\Omega_c \int_{t'-t_{ad}}^{t'} \dot{m}_w(t, r) dt}{\Omega_w \frac{m_p}{m_e}}, \quad (6)$$

for $t' > t_{ad}$ since the electrons accelerated at a time of t_{ad} earlier would have all cooled down.

2.3.2. Synchrotron spectrum

The synchrotron flux density at any given frequency can be calculated with $F_{\nu, max}$ and the spectral shape (Sari et al. 1998). Electrons are usually accelerated to a power-law distribution as $dN(\gamma_e) = C\gamma_e^{-p}d\gamma_e$, $\gamma_e > \gamma_m$ where $p = 2.5$ is the spectral index and γ_m is the minimum Lorentz factor of the electrons (Sturmer et al. 1997; Gaisser et al. 1998; Sari et al. 1998). The coefficient $C = (p-1)\gamma_m^{p-1}N_e(t')$ is obtained with $\int_{\gamma_m}^{\infty} dN(\gamma_e) = N_e(t')$. Assuming a fraction ϵ_e of the outflow's kinetic energy goes into accelerating electrons, γ_m can be calculated, based on the total energy of the accelerated electrons, as: $\gamma_m = \frac{1}{2}\epsilon_e(m_p/m_e)[(p-2)/(p-1)]\beta_w^2$.

The spectrum produced by these power-law electrons is featured with three breaking frequencies. The first breaking frequency is the characteristic frequency $\nu_m = \gamma_m^2 eB/2\pi m_e c \approx 1 \times 10^6 B_{-1} \gamma_{m,2}^2$ Hz where $\gamma_{m,2} \equiv \gamma_m/2$. The second is the self-absorption frequency ν_a , below which the emitting region is optically thick. It can be obtained by solving $\int \alpha_\nu dl \approx \alpha_\nu l = 1$ where l is the radial width of the emitting region and $\alpha_\nu \sim 10^{13} (C/\Omega_c R_{in}^2) B^{(p+2)/2} \nu^{-(p+4)/2}$ is the self-absorption

coefficient (Rybicki & Lightman 1986). Then we have:

$$\nu_a \approx 5.4 \times 10^9 \Omega_w^{-\frac{p+6}{2(p+4)}} \epsilon_{e,-1}^{\frac{2}{p+4}} \epsilon_{b,-3}^{\frac{p+2}{2(p+4)}} \gamma_{m,2}^{\frac{2(p-2)}{p+4}} \dot{m}_{w,-1}^{\frac{p+6}{2(p+4)}} \beta_{w,-1}^{\frac{p+10}{2(p+4)}} R_{in,-1}^{-\frac{p+6}{p+4}} t_{w,2}'^{\frac{2}{p+4}} \text{ [Hz]}. \quad (7)$$

where $t_{w,2}' \equiv t'/100$ days. The third is the cooling frequency ν_c , where electrons with Lorentz factor γ_c would have cooled down in the time t' . It can be obtained by solving $\gamma_c m_e c^2 = P(\gamma_c) t'$ (Sari et al. 1998), which gives $\nu_c = 1.6 \times 10^{13} B_{-1}^{-3} t_{w,2}'^{-2}$ Hz.

Figure 2 shows all the six possible spectra cases, each of which consists of three or four power law segments, and the red star marks $F_{\nu, max}$ (Granot & Sari 2002; Gao et al. 2013). Comparison of these frequencies shows that the upper right case ($\nu_m < \nu_a < \nu_c$) in Figure 2 is concerned most of the time. Finally, we smooth our analytical spectra with the following equation (Granot & Sari 2002):

$$F_\nu = F_\nu(\nu_m) \left[\left(\frac{\nu}{\nu_m} \right)^2 \exp(-s_4(\nu/\nu_m)^{2/3}) + \left(\frac{\nu}{\nu_m} \right)^{5/2} \right] \times \left[1 + \left(\frac{\nu}{\nu_a} \right)^{s_5(\beta_2 - \beta_3)} \right]^{-1/s_5}, \quad (8)$$

where $\beta_2 = 5/2$, $\beta_3 = (1-p)/2$, $s_4 = 3.63p - 1.6$ and $s_5 = 1.25 - 0.18p$.

2.4. Light curve from the shocked outflow

The radio flare from the outflow-cloud interaction would appear at $R_{in}/v_w \sim 0.1$ pc/0.1 c \sim year after TDEs. Its light curve first rises as the outflow density upstream the bow shock increases with time. Then it peaks at $t_w(R_{in})$ when the outflow's density starts declining while $N_e(t')$ remains nearly unchanged. Later, the decrease in $N_e(t')$ after t_{ad} due to the adiabatic expansion would make F_ν decrease more rapidly. The peak radio luminosity at time $t' = t_w(R_{in})$ can be crudely estimated as:

$$(\nu L_\nu)_{peak} \approx \nu_a N_e P_{\nu, max} \left(\frac{\nu_a}{\nu_m} \right)^{\frac{1-p}{2}} \approx 8 \times 10^{38} \Omega_c \Omega_w^{-\frac{19+3p}{2(p+4)}} \epsilon_{e,-1}^{\frac{3p+5}{2(p+4)}} \epsilon_{b,-3}^{\frac{4p-11}{p+4}} \dot{m}_{0,-1}^{\frac{3p+19}{2(p+4)}} \beta_{w,-1}^{\frac{7p+21}{2(p+4)}} R_{in,-1}^{-\frac{2p+22}{2(p+4)}} t_{w,2}'^{\frac{7}{p+4}} (R_{in}) \text{ [erg/s]}. \quad (9)$$

where $t_{w,2}'(R_{in}) \equiv t_w(R_{in})/100$ days. It shows that the luminosity depends most sensitively on v_w : a faster outflow would generally produce a brighter flare.

Figure 3 shows the predicted light curve from the outflow-cloud interaction. The rising timescale of

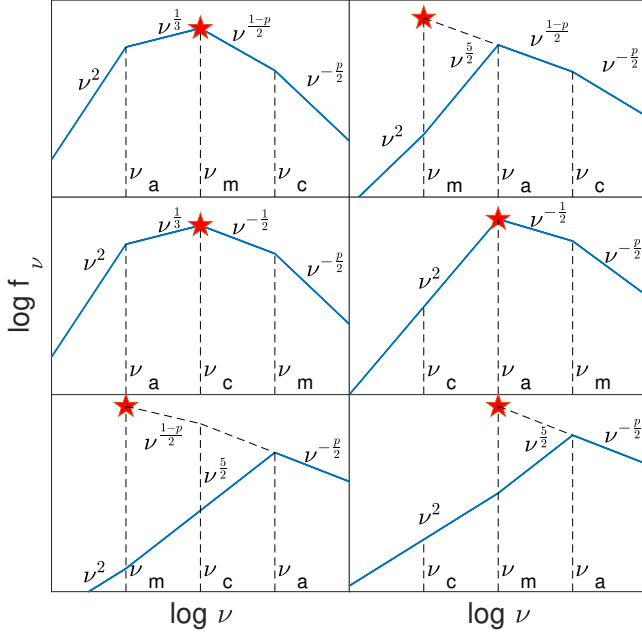


Figure 2. The possible synchrotron spectra from the shocked electrons. The spectral shape is determined by the relative ordering of the self-absorption frequency ν_a , the characteristic frequency ν_m , and the cooling frequency ν_c . The red star marks $F_{\nu,max}$.

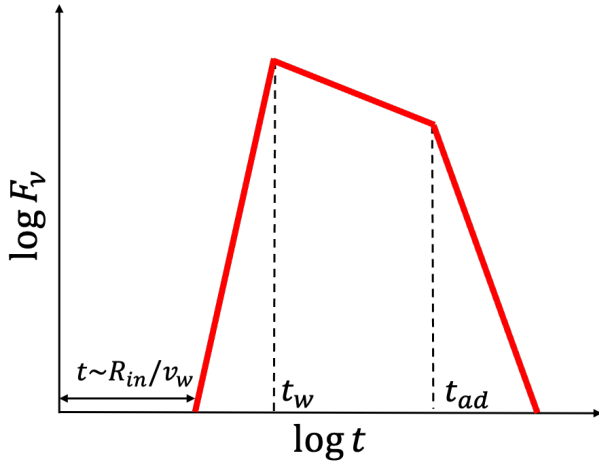


Figure 3. Sketch of the predicted radio light curve from the outflow-cloud interaction where t_w is the duration of the outflow and t_{ad} is the adiabatic cooling timescale of the shocked outflow.

$t_w(R_{in})$ is determined by the width of the outflow $\Delta(R_{in})$. A larger velocity spread of the outflow would cause a wider width, thus a shallower rise of the light curve. Since $t_w(R_{in})$ is smaller than R_{in}/v_w , the outflow-cloud interaction can reproduce the sharp rise of the light curve due to the time lag of the collision. If one were to use a power-law form t^k to fit

this rise, then the index k can be crudely estimated as $k = \log(F_{\nu,peak}/F_{\nu,ul})/\log[1+t_w/(R_{in}/v_w)] \approx 1/\log(1+\Delta_0/R_{in})$, where $F_{\nu,ul}$ is the last pre-flare observational upper limit and is generally an order of magnitude lower than the flare peak flux density $F_{\nu,peak}$. Thus, we have $k \approx 3 \sim 20$ when Δ_0/R_{in} is $0.1 \sim 1$.

3. THE OUTFLOW-CNM INTERACTION

The sweeping-up of a diffuse CNM by the outflow would produce radio emission as well. Furthermore, changes in the velocity of the outflow due to this process would affect the radiation properties from the bow shock. Here we assume a CNM density profile $n_{CNM}(r) = Ar_{-2}^{-1} \text{ cm}^{-3}$ where A is a constant and $r_{-2} \equiv r/10^{-2} \text{ pc}$, similar to the density distribution of CNM around Sgr A* (Xu et al. 2006; Gillessen et al. 2019). We model the hydrodynamic evolution of the outflow under a set of hydrodynamical equations (Huang et al. 2000) :

$$\frac{dr}{dt} = \beta_w c \quad (10)$$

$$\frac{dM}{dr} = \Omega_w r^2 n_{CNM} m_p, \quad (11)$$

$$\frac{d\beta_w}{dM} = -\frac{\beta_w(1 + \beta_w^2/4)}{m_w + M + (1 - \epsilon)(1 + \beta^2)M}, \quad (12)$$

where M is the swept CNM mass by the forward shock and ϵ describes the radiation efficiency (Dai et al. 1999).

Integrating these equations with proper initial conditions, we can obtain the hydrodynamic evolution of the outflow, and calculate the associated radiation properties from the shocked CNM according to Sari et al. (1998). The resultant radio luminosity would rise as $\nu L_\nu \propto t$, and reach its peak luminosity of

$$(\nu L_\nu)_{peak} = 1.8 \times 10^{36} m_{w,-1}^{\frac{p+11}{4(p+4)}} A_4^{\frac{5p+27}{4(p+4)}} \Omega_w^{\frac{3p+5}{4(p+4)}} \beta_{w,-1}^{\frac{17p-9}{p+4}} \epsilon_{b,-3}^{\frac{3p+5}{2(p+4)}} \epsilon_{e,-2}^{\frac{10p-7}{p+4}} \text{ [erg/s]} \quad (13)$$

at the deceleration time $t_{dec} = 3.5 \times 10^3 m_{w,-1}^{1/2} A_4^{-1/2} \Omega_w^{-1/2} \beta_{w,-1}^{-1}$ [day], when the mass of the shocked CNM equals to that of the outflow, and $A_4 \equiv A/10^4$, $m_{w,-1} = m_w/0.1 M_\odot$.

Figure 4 shows the predicted light curves at 1 GHz for different CNM density profiles. It shows that a denser CNM (i.e., a higher A) produces a brighter and earlier radio flare, while a more dilute CNM leads to a dimmer, thus maybe undetectable, flare ($\nu L_\nu < 10^{36} \text{ erg/s}$).

4. APPLICATION

In this section, we apply our model to five TDE candidates with late-time radio flares: AT2018hyz,

Table 1. Parameters for the outflow-cloud interaction model applied to the late radio flares in five TDEs, as well as those for the outflow-CNM interactions applied to the early radio flare. The multiple flares in ASASSN-15oi require five clouds (see Figure 12) while it is two clouds for AT2019azh (see Figure 8).

	CNM	Forward shock			Outflow		Cloud		Bow shock	
	A [10^3 cm^{-3}]	ϵ_e [10^{-2}]	ϵ_b [10^{-3}]	v_w [c]	m_w [$10^{-2} M_\odot$]	t_w [10^2 day]	R_{in} [10^{-1} pc]	R_c [10^{-1} pc]	ϵ_e [10^{-2}]	ϵ_b [10^{-3}]
AT 2020vwl	5.8	2	1	0.24	0.6	0.4	1.1	0.61	20	200
AT 2019azh	8.5	1	1	0.46	0.45	1.64	1.06	0.38	5	40
AT 2019azh(2)							2	0.8	20	140
IGR J12580+0134	7	1	1	0.41	4.4	0.8	4.23	1.9	12	120
AT 2018hyz	0.05	1	1	0.6	31	5.2	4.2	2.6	5	1
ASASSN-15oi(1)				0.5	3.5	0.23	0.45	0.13	1	1.5
ASASSN-15oi(2)				0.47			0.65	0.33	0.5	1
ASASSN-15oi(3)				0.44			1	0.37	3	1
ASASSN-15oi(4)				0.4			3.8	1.7	10	50
ASASSN-15oi(5)				0.36			6.4	2.5	13	100

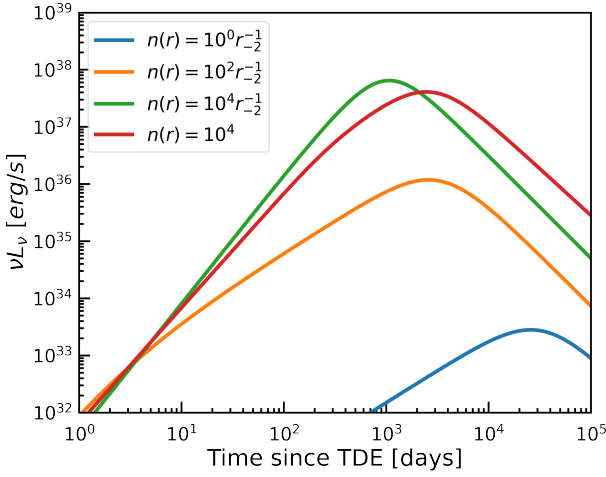


Figure 4. Predicted light curves at 1 GHz from the outflow-CNM interaction for different CNM density profile. Other parameters as $\epsilon_e = 0.01$, $\epsilon_b = 0.001$, $m_w = 0.1 M_\odot$ and $v_w = 0.3 c$.

AT2019azh, ASASSN-15oi, IGR J12580+0134 and AT2020vwl. Their radio light curves are shown in Figure 5, with peak luminosities of $10^{37} \sim 10^{39}$ erg/s.

Besides showing late-time radio flares, two events, AT2019azh and AT2020vwl, show an earlier peak ($t < 200$ days) as well. A third event, IGR J12580+0134, shows a slow decline before the late, rapid rebrightening. Noticing their apparent slow evolution, we would interpret these early flares or decline as being due to the outflow-CNM interaction. Note that the early radio flare would be missing if the CNM is dilute, which we think to be the case for the other events.

4.1. AT2020vwl

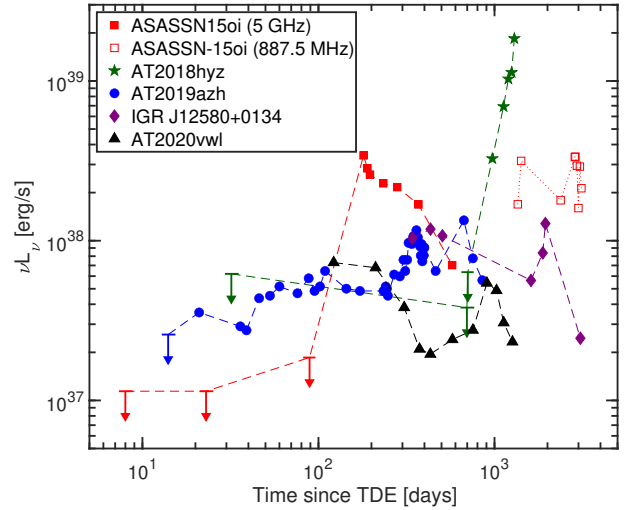


Figure 5. Light curves of TDEs with late-time radio flares: ASASSN-15oi (5 GHz, Horesh et al. 2021; 887.5 MHz Anumarlapudi et al. 2024; the data at 1,414 and 2,376 days are obtained with $f_{887.5 \text{ MHz}} = f_{3 \text{ GHz}} [887.5 \text{ MHz}/3 \text{ GHz}]^{1/3}$ for they are observed by VLASS at about 3 GHz.), AT2018hyz (5 GHz, Cendes et al. 2022), AT2019azh (15.5 GHz, Sfaradi et al. 2022; Goodwin et al. 2022), IGR J12580+0134 (1.5 GHz, Perlman et al. 2022) and AT2020vwl (5.5 GHz, Goodwin et al. 2023b, Goodwin et al. 2023a, Goodwin et al. 2024), including early upper limits.

Figure 6 shows the observed and modeled light curve at 5 GHz for AT2020vwl. The adopted parameters listed in Table 1. The green dashed line shows that the outflow-cloud interaction can generate a bright late-time radio flare after 600 days. Figure 7 shows the model fittings of spectra by the outflow-CNM and the

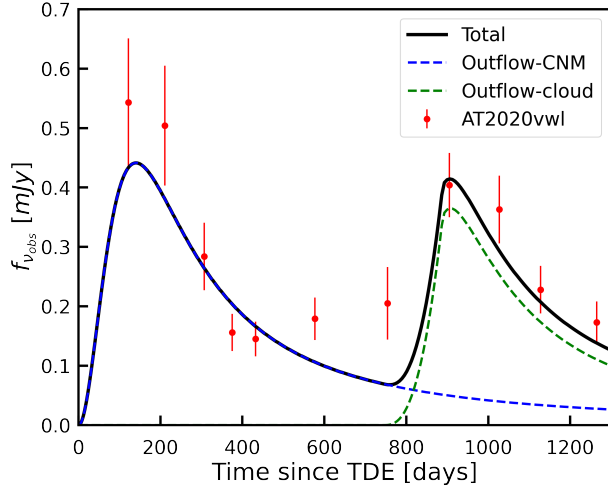


Figure 6. The observed and modeled Light curves at 5.5 GHz for AT2020vwl. Here we consider the emissions from the outflow-CNM interaction (blue dashed line), and that from the outflow-cloud interaction (green dashed line), respectively. The combined flux is shown as the black solid line.

outflow-cloud interaction. The dotted line is from the outflow-CNM interaction while the dashed line is from the outflow-cloud interaction. The solid line is the sum of them and the spectra are well explained by our model.

4.2. AT2019azh

Similar to AT2020vwl, the 15.5 GHz radio observation in AT2019azh shows an early rise of about 30 days and is followed by a late-time brighter radio flare with a peak luminosity of 10^{38} erg/s at about 350 days (Sfaradi et al. 2022). Even later ($t > 400$ days) observation at $1 \sim 10$ GHz by Goodwin et al. (2022) reveals that the light curve at 15.5 GHz would have re-brightened again at $t \sim 600$ days. These would suggest that the outflow might have collided with two clouds, one inner and the other outer in distance.

Figure 8 shows the observed and modeled light curves at 15.5 GHz for AT2019azh. The later ($t > 400$ days) observational data has been extrapolated from $1 \sim 10$ GHz to 15.5 GHz using a power-law spectral model. The overall model parameters adopted are listed in Table 1.

The outflow-CNM interaction produces a radio flare that peaks at about 100 days. Though the outflow is decelerating, its velocity is higher than $0.2 c$ while colliding with the clouds. So when the clouds are hit, with higher values (both ~ 0.1) of ϵ_b and ϵ_c , the late-time and brighter radio flares are generated. The power-law index of the temporal decay of the outflow mass rate $\dot{m}(t', r)$ determines how fast the flare decays and we found an index of 2 is preferred over $5/3$.

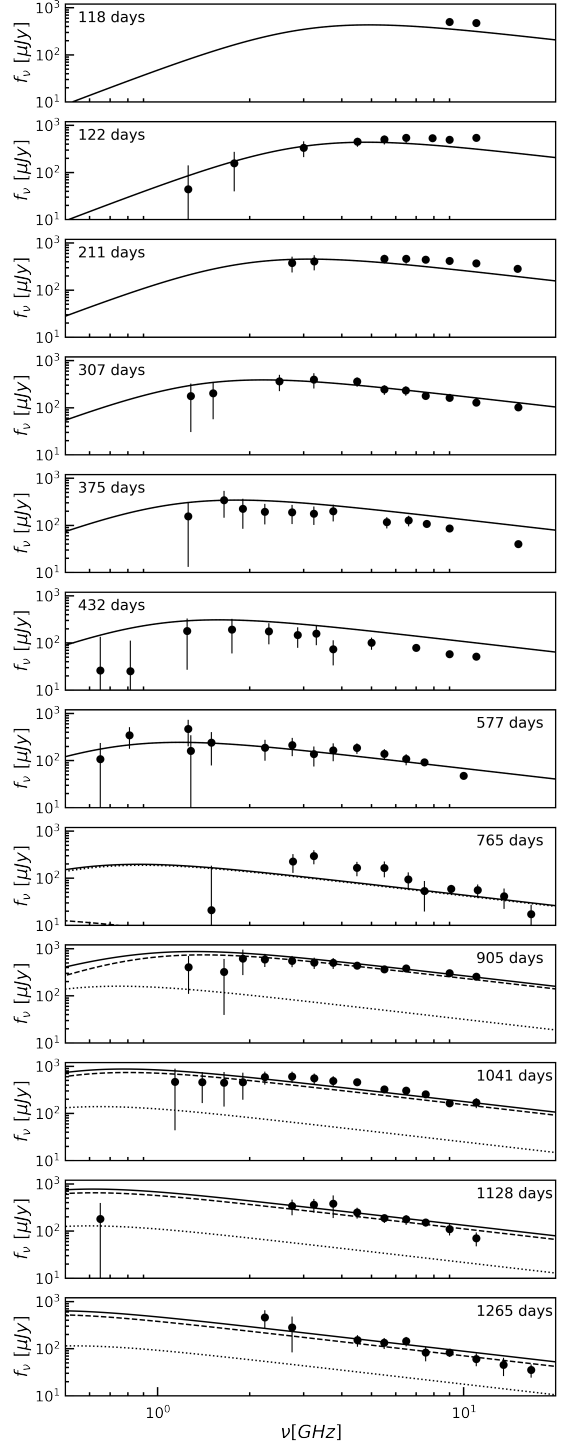


Figure 7. Model fittings of the spectra and its evolution for AT2020vwl. The radio data is from Goodwin et al. (2023b) and Goodwin et al. (2024). The early emission ($t < 900$ days) is dominated by the outflow-CNM interaction (dotted line) and the later one by the outflow-cloud interaction (dashed line). The solid line is the sum of the two emission components.

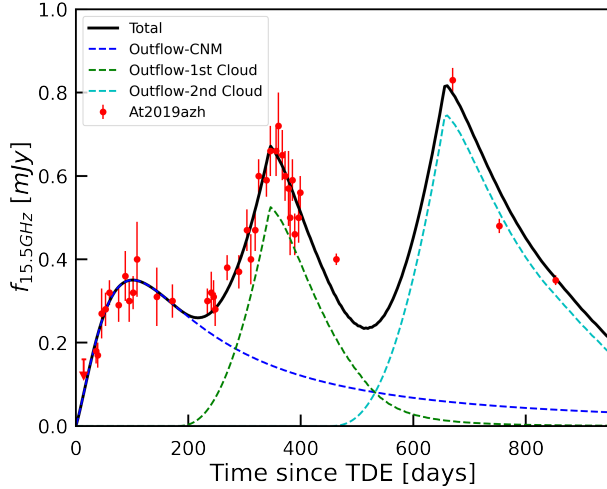


Figure 8. Same as Figure 6 but for AT2019azh at 15.5 GHz, including early upper limit. Here, two clouds are needed, for the second and the third flares, respectively.

4.3. IGR J12580+0134

The radio emission of IGR J12580+0134 was detected 350 days after the X-ray outburst and showed a decline, while later observation at 1,300 days revealed a second flare in the radio with a peak luminosity of 10^{38} erg/s (Perlman et al. 2022). Figure 9 shows the comparison of our model with the observed light curves at different frequencies (all are shifted by a factor for clarity). The parameters adopted are listed in Table 1. Here to accommodate the very steep rise of the late flare in this event, we set $a=0$ so as to limit the outflow’s radial width.

For the outflow-CNM interaction as the origin of the early decline, the light curves for $\nu < \nu_a$ would peak when ν_a crosses ν . As for the outflow-cloud interaction that explains the late flare, the predicted light curves are expected to peak at $t' = t_w(R_{in})$ because $\nu > \nu_a$ is always the case.

4.4. AT2018hyz

The late-time radio flare in AT2018hyz appeared almost 1000 days after the optical discovery with a luminosity of 10^{39} erg/s (Gomez et al. 2020; Cendes et al. 2022). Figure 10 shows the observed radio light curve and that predicted by our outflow-cloud interaction model, while Figure 11 shows the modeling of the spectra. The steep rise of the flare is well reproduced. The model also shows a rapid decay after the peak of the flare, if there is no additional outflow-cloud interaction.

The early radio non-detection of AT2018hyz, with a luminosity upper limit of $\nu L_\nu < 6 \times 10^{37}$ erg/s at $t = 700$ days, hints at a very dilute CNM (see Section 3). Simply requiring that $(\nu L_\nu)_{peak}$ of the outflow-CNM interaction be below this upper limit, that would mean $A < 430$ ac-

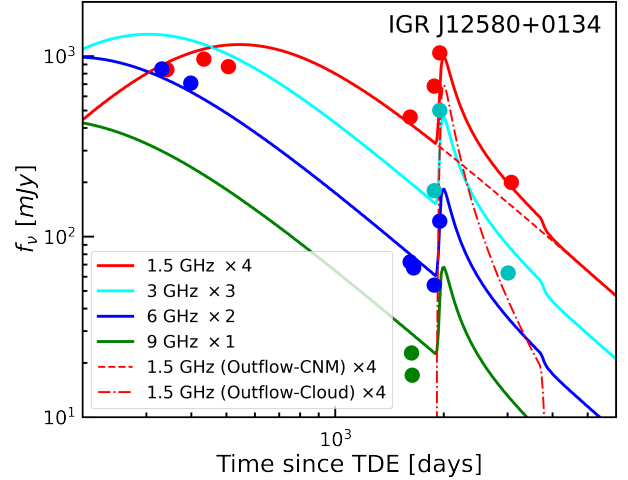


Figure 9. Same as Figure 6 but for IGRJ12580+0134 at different frequencies.

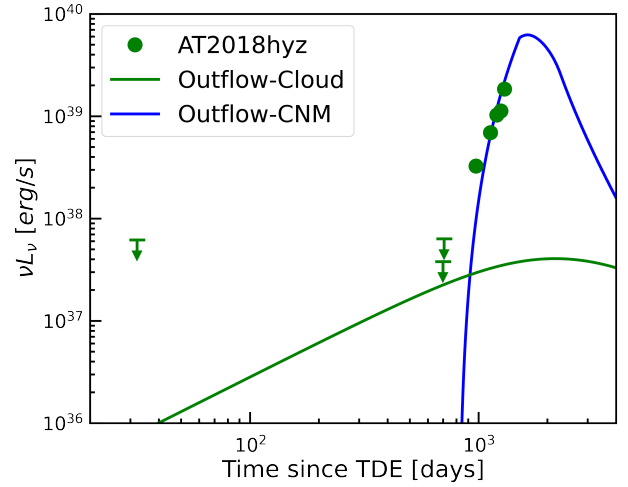


Figure 10. The observed and modeled light curves of AT2018hyz at 5 GHz. The green line (setting $A = 50$) is one of the possible light curves from the outflow-CNM interaction that are consistent with the early non-detection upper limits.

ording to Eq. (13), with all other parameters adopting values given from fitting the late radio flare. Note that the observed frequency in AT2018hyz may not be equal to the spectral peak frequency (usually ν_a), so this constraint on A might be very crude. Alternatively, we can numerically calculate the light curve from the shocked CNM and compare it with the early non-detections. We tried various values of A and found that $A = 50$ can give a result consistent with the data, which is shown in the green line in Figure 10. Therefore, $A < 50$ is required for AT2018hyz.

4.5. ASASSN-15oi

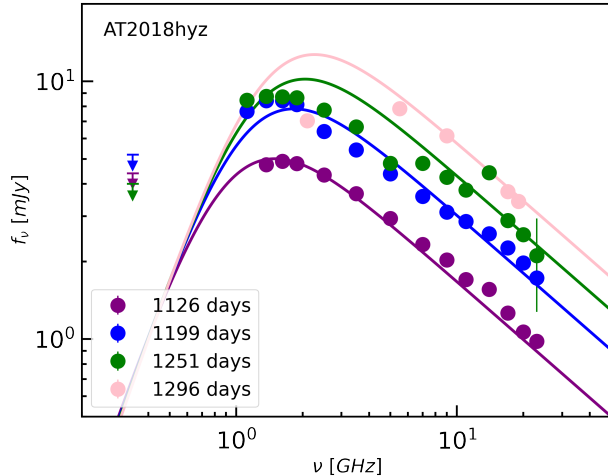


Figure 11. Model fittings of the temporal evolution of the spectra from the outflow-cloud interaction for AT2018hzy, including upper limits.

Multiple radio flares are observed in ASASSN-15oi (Horesh et al. 2021; Anumarlapudi et al. 2024), thus additional clouds are needed in our model. As for the flare before 700 days, apart from the sudden change of the peak frequency at the 4th observation, the complex evolution of the light curve (fast - slow - fast decay) is not predicted by our model (see Figure 5). Thus, we suspect that the flare before 700 days comes from the interaction of the outflow with at least two closely located clouds. Overall, we consider these multiple late-time radio flares are from the interaction of the outflow with at least five giant clouds at different distances. Figure 12 shows the modeling of the light curve, and Figure 13 shows the spectra comparison between the observed and the predicted. The adopted parameter values for these five collisions are shown in Table 1.

Here among these collisions, the radial width $t_w(r)$ increases with distance due to the radial expansion of the outflow (see Section 2.2). After each previous cloud collision, taking into account that part of the outflow's kinetic energy is dissipated, we adopt a reduced value of v_w for the next collision. In addition, as the outflow moves outwards and the density of the outflow decreases, we found that much higher ϵ_e and ϵ_b are needed for the last two clouds than the inner clouds to account for the later but brighter flares.

The adopted velocities ($v_w \sim 0.5c$) for ASASSN-15oi and AT2018hzy are higher than other events because of their brighter luminosities. Simulations (Dai et al. 2018; Bu et al. 2023b) show that the outflow has a wide range of v_w about $0.1 \sim 0.8 c$, depending sensitively on the inclination angle. Thus, our values are in a reasonable regime.

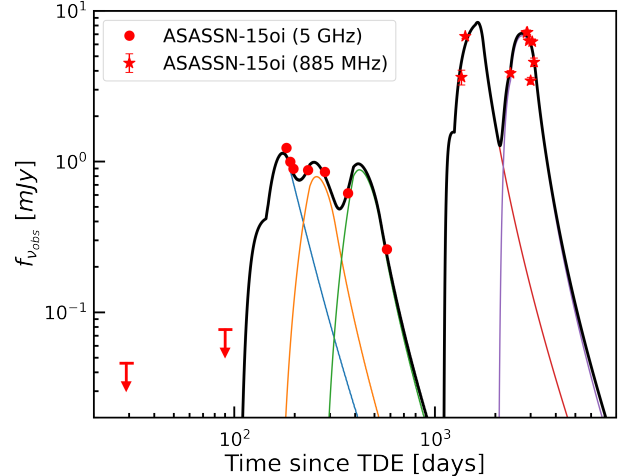


Figure 12. The modeling of radio light curves at 5 GHz and 885 MHz for ASASSN-15oi, including early upper limits. The emission is from the interaction of the outflow with five giant clouds at different distances. The different color thin lines mark the light curve from different clouds while the thick black line marks the total light curve. The parameters adopted are listed in Table 1.

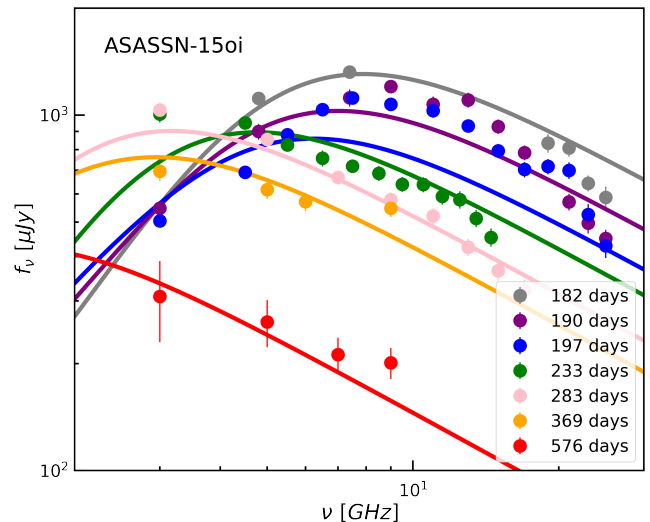


Figure 13. Model fittings of the temporal evolution of the spectra from the outflow-clouds interaction for ASASSN-15oi.

5. DISCUSSION

Here we discuss an off-axis jet, which can produce the step rise as observed and is proposed to explain these late radio flares (Matsumoto & Piran 2023; Sfaradi et al. 2024). We also consider the possible accompanying X-ray emission from the outflow-cloud interaction (Mou et al. 2021; Zhuang & Shen 2021), and compare it with observations.

5.1. An off-axis jet

A TDE might generate a relativistic jet (Frank & Rees 1976; De Colle et al. 2012; Metzger et al. 2012). The shock interaction between the relativistic jet and the CNM powers non-thermal radio synchrotron radiation (Giannios & Metzger 2011). The radio signal is beamed away from the observers initially if we are not located within the initial jet aperture θ_j (an off-axis jet). As the jet decelerates, the emission from the jet becomes detectable to observers at larger viewing angles θ_{obs} , producing a steep rise as $f_\nu \propto t^{(15-3p)/2}$ for $\nu > \max(\nu_m, \nu_a)$ (Rhoads 1999; Granot et al. 2002).

In the off-axis jet scenario, the radio would peak at a time t_p with a peak luminosity νL_ν ($\nu = 1$ GHz) as (Nakar et al. 2002; Gottlieb et al. 2019):

$$t_p = 60 n_0^{-1/3} E_{52}^{1/3} \left(\frac{\theta_{obs} - \theta_j}{15^\circ} \right)^2 [\text{day}] \quad (14)$$

$$\nu L_\nu \approx 1.1 \times 10^{38} \epsilon_{e,-1}^{p-1} \epsilon_{b,-3}^{(p+1)/4} n_0^{(p+1)/4} E_{52} \left(\frac{\theta_{obs}}{20^\circ} \right)^{-2p} \quad (15)$$

[erg/s]

where E_{52} is the energy of the jet in units of 10^{52} erg; n_0 is the uniform ambient density in cm^{-3} . The equations reveal that a flare with a peak time of about 1,000 days and a peak luminosity of 10^{39} erg/s is possible.

Lei et al. (2016) find that the the data before 1,000 days in IGR J12580+0134 are consistent with an off-axis relativistic jet. Besides, Sfaradi et al. (2024) also find that the off-axis jet model can explain the full set of radio observations of AT2018hyz. However, the delayed radio flare seen in ASASSN-15oi cannot be explained by such a model, as Horesh et al. (2021) find that its best-fit parameters vary substantially between each epoch and no numerical solution can account for both the initial steep flux rise, and the complex spectral and temporal evolution. Sato et al. (2024) find that a structured two-component jet (a relativistic inner component and trans-relativistic outer component), instead of the one-component jet, can explain the radio data of ASASSN-15oi before 1,400 days, as well as ASASSN-1eae, AT2018hyz and AT2019dsg. Nevertheless, the latest observed flux variation after 1,400 days in ASASSN-15oi is unlikely to be explained by this model.

5.2. X-ray emission from the outflow-cloud interaction

The interaction of outflow with a cloud can also drive a cloud shock that propagates into the cloud (McKee & Cowie 1975). The cloud shock's velocity is $\beta_{sc} = \beta_w \chi^{-1/2} \approx 0.003 \beta_{w,-1} \chi_3^{-1/2}$, where $\chi_3 = (n_c/n_w)/10^3$ is the density ratio and n_c is the cloud's gas number density. The shocked cloud material's temperature is $T_{sc} = 3m_H c^2 \beta_{sc}^2 / 16k \approx 6 \times 10^6 \beta_{w,-1}^2 \chi_3^{-1}$ K, which

means that the shocked cloud radiates in X-rays. Below, we estimate its luminosity.

The internal energy gained by the shocked cloud per unit time is $\dot{E}_{c,th} = \frac{9}{32} \rho_c r^2 v_{sc}^3 \Omega_c$, and the energy conversion efficiency is $\eta = \dot{E}_{c,th} / L_w \approx 2\% \frac{\Omega_c}{\Omega_w} \chi_3^{-1/2}$ where the L_w is the kinetic luminosity of the outflow (Mou & Wang 2021). In addition, Chen & Wang (2023) found that the thermal conduction inside the cloud can play a crucial role in increasing the cloud's radiation, and up to 5~10% of the kinetic energy of the outflow impacting the cloud could be converted into radiation. In this case, one has $\eta = 5 \sim 10\% \Omega_c / \Omega_w$.

This energy will be radiated out. The radiative cooling timescale is $t_{cool} = 0.69kT_{sc}/n_c\Lambda(T_{sc}) \approx 5 \times 10^6 T_{sc,7}^{1/2} n_{c,7}^{-1}$ s where $T_{sc,7} \equiv T_{sc}/10^7$ K, $n_{c,7} \equiv n_c/10^7 \text{ cm}^{-3}$ and $\Lambda(T) \approx 6 \times 10^{-27} T^{1/2}$ [erg cm^3/s] is the temperature-dependent volume cooling function (Raymond et al. 1976; Blondin et al. 1998; Lin & Murray 2000).

For $t_{cool} < t_w$, the cooling is so strong that the internal energy of the shocked cloud is rapidly lost in radiation. Then, the X-ray luminosity is $\eta L_w(t)$ which would peak at $t' = t_w(r)$ with a peak luminosity of

$$L_X \approx 10^{41} \Omega_{c,-1} \Omega_w^{-1} n_{w,4}^{1/2} n_{c,7}^{-1/2} L_{w,44} \text{ erg/s} \quad (16)$$

where $L_{w,44} \equiv L_w/10^{44}$ erg/s.

For $t_{cool} > t_w$, the peak luminosity can be estimated as $L_X = \eta E_w / t_{cool}$ or

$$L_X \approx 10^{40} E_{w,50} \Omega_{c,-1} n_{c,7}^{7/22} n_{w,4}^{1/2} \beta_{w,-1}^{-3/11} \dot{m}_{0,-1}^{-3/11} \Omega_w^{-17/11} R_{in,-1}^{6/11} t_{w,2}^{-5/11} \text{ [erg/s]} \quad (17)$$

at a peak time $t' = t_{cool}$ or

$$t_{cool} \approx 100 n_{c,7}^{-9/11} \dot{m}_{0,-1}^{3/11} \Omega_w^{6/11} R_{in,-1}^{-6/11} \beta_{w,-1}^{3/11} t_{w,2}^{5/11} \text{ [day]} \quad (18)$$

where $E_w = E_{w,50} \times 10^{50}$ erg is the total energy of the outflow.

5.2.1. Comparison with observations

Below we check the above with the events that show possible X-ray flares accompanying the late-time radio flares. We found no report of X-ray observation for IGR J12580+0134 and AT2020vwl near the times of their late radio flares, while there is only one observational X-ray data for AT2018hyz (Cendes et al. 2022). For AT2019azh (Hinkle et al. 2021) and ASASSN-15oi (Gezari et al. 2017; Hajela et al. 2024), both have sufficient X-ray data detected accompanying the radio flare, and their X-ray light curves are shown in Figure 14 and Figure 15, respectively.

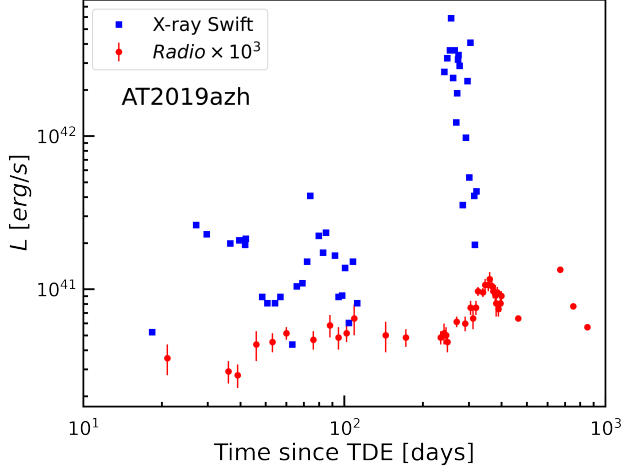


Figure 14. The X-ray and radio light curves for AT2019azh. The X-ray data is from [Hinkle et al. \(2021\)](#).

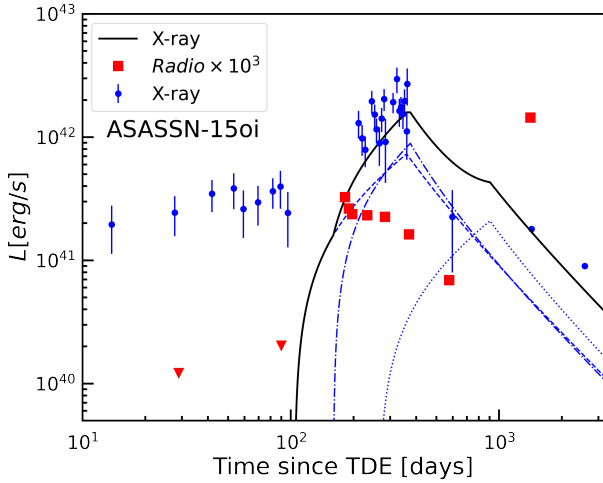


Figure 15. The X-ray and radio light curves for ASASSN-15oi. The X-ray data is from [Gezari et al. \(2017\)](#) and [Hajela et al. \(2024\)](#). The dashed, dotted-dashed and dotted lines are X-ray emission from the interaction of the outflow with the 1st, 2nd, and 3rd clouds, respectively, while the black line is the total emission.

For AT2018hyz, its X-ray luminosity remains nearly constant at 10^{41} erg/s up to 250 days ([Gomez et al. 2020](#); [Hung et al. 2020](#)). The latest observation at $t = 1253$ days by [Cendes et al. \(2022\)](#) shows a luminosity of 5×10^{40} erg/s. Our late radio flare modeling for AT2018hyz has found that the collision occurred at $t = 800$ days, with $t_w(R_{in}) \sim 700$ days. Then with all those parameters and using Eq. (16), we found that $n_c = 10^8 \text{ cm}^{-3}$ (corresponding to a cloud mass of $\sim 10^5 M_\odot$) can produce an X-ray flare in the $t_w > t_{cool}$ regime with $L_X \sim 7 \times 10^{40}$ erg/s at $t = 1500$ days. The X-ray luminosity from the shocked cloud is still rising at $t = 1250$ day, hence is consistent with the observation.

For AT2019azh, its late-time X-ray shows a peak luminosity of $L_X \approx 10^{42}$ erg/s and it peaks earlier than the radio at least 100 days ahead. However, according to Eqs. (16-18), the predicted X-ray peak time is $\approx \max(t_w, t_{cool})$, which is unlikely earlier than the radio that peaks at t_w . On the other hand, we found that adopting $n_c = 10^7 \text{ cm}^{-3}$ will result in an X-ray flare in the $t_w > t_{cool}$ regime that peaks at 350 days with $L_X \approx 10^{40}$ erg/s, much lower than the observed. Thus, the late X-ray flare of AT2019azh may not come from the outflow-cloud interaction and it may be related to the on-going SMBH accretion instead.

For ASASSN-15oi, the late-time accompanying X-ray peaks at about 350 days with $L_X \approx 10^{42}$ erg/s, and then shows a slow decline to $\sim 10^{41}$ erg/s. The X-ray peak time is ~ 300 days later than the radio. Our modeling has found that three clouds are required for the radio emission before 600 days. We calculate the X-ray light curves from the collisions of the outflow with each cloud, simply adopting a linear rise and exponential decay light curve shape. We found that the observed X-ray may be accounted for by summing up the emission from the three collisions (see the solid black line in Figure 15). Here, $n_c = 10^{6.8} \text{ cm}^{-3}$ is adopted for all the three clouds, corresponding to cloud masses of 1, 20 and 30 M_\odot , respectively.

6. CONCLUSION

In recent years, radio observation of some TDEs reveals flares only at a late time ($10^2 \sim 10^3$ days after TDE discovery), such as in ASASSN-15oi and AT2018hyz, both of which have a radio luminosity of about 10^{39} erg/s. Due to the rapid evolution of light curves, some of these late-time radio flares are difficult to be explained by the conventional outflow-CNM interaction, of which the steepest evolution is $f_\nu \propto t^3$ ([Metzger et al. 2012](#); [Krolik et al. 2016](#); [Alexander et al. 2020](#)) while observation requires a temporal power-law steeper than t^4 .

A variety of explanations have been proposed for these late-time radio flares such as a delayed launch of the outflow ([Cendes et al. 2023](#)), a misaligned precessing jet ([Teboul & Metzger 2023](#)), an off-axis jet ([Matsumoto & Piran 2023](#); [Sfaradi et al. 2024](#)), and a piecewise power-law distribution of CNM ([Matsumoto & Piran 2024](#)).

In this paper, we developed the outflow-cloud interaction model for the late-time radio flares. This collision forms a bow shock, and the late-time radio synchrotron emission is produced from the shocked outflow. We found it is capable of generating bright radio flares years after TDE with a luminosity of 10^{39} erg/s, and can explain the large delay, the sharpness of the rise and the multiplicity of the late radio flares.

The model is applied to five TDE candidates and our model can well explain the observed data, including the multiple late-time flares such as seen in ASASSN-15oi, when the outflow impacts multiple clouds. The inferred outflow velocity ranges from $0.2c$ to $0.6c$ with a mass outflow rate of about $0.01 \sim 0.1 M_{\odot}/\text{year}$. The corresponding kinetic luminosity of these outflows is about $10^{44\sim 45}$ erg/s which is consistent with the simulation (Curd & Narayan 2019; Bu et al. 2023b,a), and the total kinetic energy of the outflow is $10^{50} \sim 10^{51}$ erg with a total mass of about $0.01 \sim 0.1 M_{\odot}$. The distances (~ 0.1 pc) and the number of clouds required are compatible with observations (Mezger et al. 1996; Christopher et al. 2005).

Our model may be tested by the accompanied X-ray or dust echo emission component. Here in this paper, with the parameters obtained by the radio modeling, we found that the X-ray emission in ASASSN-15oi and AT2018hyz can be explained by the shocked clouds, while the X-ray in AT2019azh may come directly from some on-going accretion. In addition, there may be lots

of dust in the torus as well, such that the UV emission from the TDE's early accretion may be absorbed and reprocessed into the infrared (Lu et al. 2016).

With more late-time radio flares by future observation, we will examine whether our model can be applied to these events and offer constraints on the outflow to help better understand TDEs. In addition, they can also be used as a tool to study the circumnuclear environment.

ACKNOWLEDGEMENTS

We thank the anonymous referee for many constructive comments and suggestions that helped improve the quality of this paper. We thank Adelle Goodwin for helpful comments. R. Shen and J. Zhuang are supported by National Natural Science Foundation of China (grants 12073091 and 12261141691) and by the Strategic Priority Research Program of Chinese Academy of Sciences (grant XDB0550200). G. Mou is supported by the NSFC (No.12133007).

REFERENCES

- Alexander, K. D., van Velzen, S., Horesh, A., & Zauderer, B. A. 2020, *SSRv*, 216, 81, doi: [10.1007/s11214-020-00702-w](https://doi.org/10.1007/s11214-020-00702-w)
- Anumarlapudi, A., Kaplan, D., Dobie, D., et al. 2024, *The Astronomer's Telegram*, 16502, 1
- Armijos-Abendaño, J., López, E., Llerena, M., & Logan, C. H. A. 2022, *MNRAS*, 514, 1535, doi: [10.1093/mnras/stac1442](https://doi.org/10.1093/mnras/stac1442)
- Barkov, M. V., Lyutikov, M., & Khangulyan, D. 2019, *MNRAS*, 484, 4760, doi: [10.1093/mnras/stz213](https://doi.org/10.1093/mnras/stz213)
- Barniol Duran, R., Nakar, E., & Piran, T. 2013, *ApJ*, 772, 78, doi: [10.1088/0004-637X/772/1/78](https://doi.org/10.1088/0004-637X/772/1/78)
- Beniamini, P., Nava, L., & Piran, T. 2016, *MNRAS*, 461, 51, doi: [10.1093/mnras/stw1331](https://doi.org/10.1093/mnras/stw1331)
- Blandford, R. D., & Znajek, R. L. 1977, *MNRAS*, 179, 433, doi: [10.1093/mnras/179.3.433](https://doi.org/10.1093/mnras/179.3.433)
- Blondin, J. M., Wright, E. B., Borkowski, K. J., & Reynolds, S. P. 1998, *ApJ*, 500, 342, doi: [10.1086/305708](https://doi.org/10.1086/305708)
- Bloom, J. S., Giannios, D., Metzger, B. D., et al. 2011, *Science*, 333, 203, doi: [10.1126/science.1207150](https://doi.org/10.1126/science.1207150)
- Bu, D.-F., Chen, L., Mou, G., Qiao, E., & Yang, X.-H. 2023a, *MNRAS*, 521, 4180, doi: [10.1093/mnras/stad804](https://doi.org/10.1093/mnras/stad804)
- Bu, D.-F., Qiao, E., & Yang, X.-H. 2023b, *MNRAS*, 523, 4136, doi: [10.1093/mnras/stad1696](https://doi.org/10.1093/mnras/stad1696)
- Burrows, D. N., Kennea, J. A., Ghisellini, G., et al. 2011, *Nature*, 476, 421, doi: [10.1038/nature10374](https://doi.org/10.1038/nature10374)
- Cendes, Y., Berger, E., Alexander, K. D., et al. 2022, *ApJ*, 938, 28, doi: [10.3847/1538-4357/ac88d0](https://doi.org/10.3847/1538-4357/ac88d0)
- . 2023, arXiv e-prints, arXiv:2308.13595, doi: [10.48550/arXiv.2308.13595](https://doi.org/10.48550/arXiv.2308.13595)
- Chen, J., & Wang, W. 2023, *MNRAS*, 518, 5163, doi: [10.1093/mnras/stac3409](https://doi.org/10.1093/mnras/stac3409)
- Chevalier, R. A. 1998, *ApJ*, 499, 810, doi: [10.1086/305676](https://doi.org/10.1086/305676)
- Christopher, M. H., Scoville, N. Z., Stolovy, S. R., & Yun, M. S. 2005, *ApJ*, 622, 346, doi: [10.1086/427911](https://doi.org/10.1086/427911)
- Curd, B., & Narayan, R. 2019, *MNRAS*, 483, 565, doi: [10.1093/mnras/sty3134](https://doi.org/10.1093/mnras/sty3134)
- Dai, L., McKinney, J. C., Roth, N., Ramirez-Ruiz, E., & Miller, M. C. 2018, *ApJL*, 859, L20, doi: [10.3847/2041-8213/aab429](https://doi.org/10.3847/2041-8213/aab429)
- Dai, Z. G., Huang, Y. F., & Lu, T. 1999, *ApJ*, 520, 634, doi: [10.1086/307463](https://doi.org/10.1086/307463)
- De Colle, F., Guillochon, J., Naiman, J., & Ramirez-Ruiz, E. 2012, *ApJ*, 760, 103, doi: [10.1088/0004-637X/760/2/103](https://doi.org/10.1088/0004-637X/760/2/103)
- Ferrarese, L., & Ford, H. 2005, *SSRv*, 116, 523, doi: [10.1007/s11214-005-3947-6](https://doi.org/10.1007/s11214-005-3947-6)
- Frank, J., & Rees, M. J. 1976, *MNRAS*, 176, 633, doi: [10.1093/mnras/176.3.633](https://doi.org/10.1093/mnras/176.3.633)
- Gaisser, T. K., Protheroe, R. J., & Stanev, T. 1998, *ApJ*, 492, 219, doi: [10.1086/305011](https://doi.org/10.1086/305011)
- Gao, H., Lei, W.-H., Wu, X.-F., & Zhang, B. 2013, *MNRAS*, 435, 2520, doi: [10.1093/mnras/stt1461](https://doi.org/10.1093/mnras/stt1461)

- Gezari, S., Cenko, S. B., & Arcavi, I. 2017, *ApJL*, 851, L47, doi: [10.3847/2041-8213/aaa0c2](https://doi.org/10.3847/2041-8213/aaa0c2)
- Giannios, D., & Metzger, B. D. 2011, *MNRAS*, 416, 2102, doi: [10.1111/j.1365-2966.2011.19188.x](https://doi.org/10.1111/j.1365-2966.2011.19188.x)
- Gillessen, S., Plewa, P. M., Widmann, F., et al. 2019, *ApJ*, 871, 126, doi: [10.3847/1538-4357/aaf4f8](https://doi.org/10.3847/1538-4357/aaf4f8)
- Gomez, S., Nicholl, M., Short, P., et al. 2020, *MNRAS*, 497, 1925, doi: [10.1093/mnras/staa2099](https://doi.org/10.1093/mnras/staa2099)
- Goodwin, A., Miller-Jones, J., Alexander, K. D., et al. 2023a, *The Astronomer's Telegram*, 16165, 1
- Goodwin, A. J., van Velzen, S., Miller-Jones, J. C. A., et al. 2022, *MNRAS*, 511, 5328, doi: [10.1093/mnras/stac333](https://doi.org/10.1093/mnras/stac333)
- Goodwin, A. J., Alexander, K. D., Miller-Jones, J. C. A., et al. 2023b, *MNRAS*, doi: [10.1093/mnras/stad1258](https://doi.org/10.1093/mnras/stad1258)
- Goodwin, A. J., Mummery, A., Laskar, T., et al. 2024, arXiv e-prints, arXiv:2410.18665, doi: [10.48550/arXiv.2410.18665](https://doi.org/10.48550/arXiv.2410.18665)
- Gottlieb, O., Nakar, E., & Piran, T. 2019, *MNRAS*, 488, 2405, doi: [10.1093/mnras/stz1906](https://doi.org/10.1093/mnras/stz1906)
- Granot, J., Panaitescu, A., Kumar, P., & Woosley, S. E. 2002, *ApJL*, 570, L61, doi: [10.1086/340991](https://doi.org/10.1086/340991)
- Granot, J., & Sari, R. 2002, *ApJ*, 568, 820, doi: [10.1086/338966](https://doi.org/10.1086/338966)
- Granot, J., & van der Horst, A. J. 2014, *PASA*, 31, e008, doi: [10.1017/pasa.2013.44](https://doi.org/10.1017/pasa.2013.44)
- Guillochon, J., McCourt, M., Chen, X., Johnson, M. D., & Berger, E. 2016, *ApJ*, 822, 48, doi: [10.3847/0004-637X/822/1/48](https://doi.org/10.3847/0004-637X/822/1/48)
- Guillochon, J., & Ramirez-Ruiz, E. 2013, *ApJ*, 767, 25, doi: [10.1088/0004-637X/767/1/25](https://doi.org/10.1088/0004-637X/767/1/25)
- Guolo, M., Gezari, S., Yao, Y., et al. 2023, arXiv e-prints, arXiv:2308.13019, doi: [10.48550/arXiv.2308.13019](https://doi.org/10.48550/arXiv.2308.13019)
- Hajela, A., Alexander, K. D., Margutti, R., et al. 2024, arXiv e-prints, arXiv:2407.19019, doi: [10.48550/arXiv.2407.19019](https://doi.org/10.48550/arXiv.2407.19019)
- Hinkle, J. T., Holoien, T. W. S., Auchettl, K., et al. 2021, *MNRAS*, 500, 1673, doi: [10.1093/mnras/staa3170](https://doi.org/10.1093/mnras/staa3170)
- Horesh, A., Cenko, S. B., & Arcavi, I. 2021, *Nature Astronomy*, 5, 491, doi: [10.1038/s41550-021-01300-8](https://doi.org/10.1038/s41550-021-01300-8)
- Huang, Y. F., Gou, L. J., Dai, Z. G., & Lu, T. 2000, *ApJ*, 543, 90, doi: [10.1086/317076](https://doi.org/10.1086/317076)
- Hung, T., Foley, R. J., Ramirez-Ruiz, E., et al. 2020, *ApJ*, 903, 31, doi: [10.3847/1538-4357/abb606](https://doi.org/10.3847/1538-4357/abb606)
- Krolik, J., Piran, T., Svirski, G., & Cheng, R. M. 2016, *ApJ*, 827, 127, doi: [10.3847/0004-637X/827/2/127](https://doi.org/10.3847/0004-637X/827/2/127)
- Lei, W.-H., Yuan, Q., Zhang, B., & Wang, D. 2016, *ApJ*, 816, 20, doi: [10.3847/0004-637X/816/1/20](https://doi.org/10.3847/0004-637X/816/1/20)
- Lei, X., Wu, Q., Li, H., et al. 2024, arXiv e-prints, arXiv:2410.20127, doi: [10.48550/arXiv.2410.20127](https://doi.org/10.48550/arXiv.2410.20127)
- Lin, D. N. C., & Murray, S. D. 2000, *ApJ*, 540, 170, doi: [10.1086/309317](https://doi.org/10.1086/309317)
- Lu, W., & Bonnerot, C. 2020, *MNRAS*, 492, 686, doi: [10.1093/mnras/stz3405](https://doi.org/10.1093/mnras/stz3405)
- Lu, W., Kumar, P., & Evans, N. J. 2016, *MNRAS*, 458, 575, doi: [10.1093/mnras/stw307](https://doi.org/10.1093/mnras/stw307)
- Matsumoto, T., & Piran, T. 2023, *MNRAS*, 522, 4565, doi: [10.1093/mnras/stad1269](https://doi.org/10.1093/mnras/stad1269)
- . 2024, arXiv e-prints, arXiv:2404.15966, doi: [10.48550/arXiv.2404.15966](https://doi.org/10.48550/arXiv.2404.15966)
- McKee, C. F., & Cowie, L. L. 1975, *ApJ*, 195, 715, doi: [10.1086/153373](https://doi.org/10.1086/153373)
- Metzger, B. D., Giannios, D., & Mimica, P. 2012, *MNRAS*, 420, 3528, doi: [10.1111/j.1365-2966.2011.20273.x](https://doi.org/10.1111/j.1365-2966.2011.20273.x)
- Mezger, P. G., Duschl, W. J., & Zylka, R. 1996, *A&A Rv*, 7, 289, doi: [10.1007/s001590050007](https://doi.org/10.1007/s001590050007)
- Mou, G., Wang, T., Wang, W., & Yang, J. 2022, *MNRAS*, 510, 3650, doi: [10.1093/mnras/stab3742](https://doi.org/10.1093/mnras/stab3742)
- Mou, G., & Wang, W. 2021, *MNRAS*, 507, 1684, doi: [10.1093/mnras/stab2261](https://doi.org/10.1093/mnras/stab2261)
- Mou, G., Dou, L., Jiang, N., et al. 2021, *ApJ*, 908, 197, doi: [10.3847/1538-4357/abd475](https://doi.org/10.3847/1538-4357/abd475)
- Nakar, E., Piran, T., & Granot, J. 2002, *ApJ*, 579, 699, doi: [10.1086/342791](https://doi.org/10.1086/342791)
- Perlman, E. S., Meyer, E. T., Wang, Q. D., et al. 2022, *ApJ*, 925, 143, doi: [10.3847/1538-4357/ac3bba](https://doi.org/10.3847/1538-4357/ac3bba)
- Phinney, E. S. 1989, in *The Center of the Galaxy*, ed. M. Morris, Vol. 136, 543
- Raymond, J. C., Cox, D. P., & Smith, B. W. 1976, *ApJ*, 204, 290, doi: [10.1086/154170](https://doi.org/10.1086/154170)
- Rees, M. J. 1988, *Nature*, 333, 523, doi: [10.1038/333523a0](https://doi.org/10.1038/333523a0)
- Rhoads, J. E. 1999, *ApJ*, 525, 737, doi: [10.1086/307907](https://doi.org/10.1086/307907)
- Rybicki, G. B., & Lightman, A. P. 1986, *Radiative Processes in Astrophysics*
- Santana, R., Barniol Duran, R., & Kumar, P. 2014, *ApJ*, 785, 29, doi: [10.1088/0004-637X/785/1/29](https://doi.org/10.1088/0004-637X/785/1/29)
- Sari, R., Piran, T., & Narayan, R. 1998, *ApJL*, 497, L17, doi: [10.1086/311269](https://doi.org/10.1086/311269)
- Sato, Y., Murase, K., Bhattacharya, M., et al. 2024, arXiv e-prints, arXiv:2404.13326, doi: [10.48550/arXiv.2404.13326](https://doi.org/10.48550/arXiv.2404.13326)
- Sfaradi, I., Horesh, A., Fender, R., et al. 2022, *ApJ*, 933, 176, doi: [10.3847/1538-4357/ac74bc](https://doi.org/10.3847/1538-4357/ac74bc)
- Sfaradi, I., Beniamini, P., Horesh, A., et al. 2024, *MNRAS*, 527, 7672, doi: [10.1093/mnras/stad3717](https://doi.org/10.1093/mnras/stad3717)
- Strubbe, L. E., & Quataert, E. 2009, *MNRAS*, 400, 2070, doi: [10.1111/j.1365-2966.2009.15599.x](https://doi.org/10.1111/j.1365-2966.2009.15599.x)
- Sturmer, S. J., Skibo, J. G., Dermer, C. D., & Mattox, J. R. 1997, *ApJ*, 490, 619, doi: [10.1086/304894](https://doi.org/10.1086/304894)

- Tchekhovskoy, A., Narayan, R., & McKinney, J. C. 2011, MNRAS, 418, L79, doi: [10.1111/j.1745-3933.2011.01147.x](https://doi.org/10.1111/j.1745-3933.2011.01147.x)
- Teboul, O., & Metzger, B. D. 2023, ApJL, 957, L9, doi: [10.3847/2041-8213/ad0037](https://doi.org/10.3847/2041-8213/ad0037)
- Wu, H.-J., Mou, G., Wang, K., Wang, W., & Li, Z. 2022, MNRAS, 514, 4406, doi: [10.1093/mnras/stac1621](https://doi.org/10.1093/mnras/stac1621)
- Xu, Y.-D., Narayan, R., Quataert, E., Yuan, F., & Baganoff, F. K. 2006, ApJ, 640, 319, doi: [10.1086/499932](https://doi.org/10.1086/499932)
- Yalinewich, A., Steinberg, E., Piran, T., & Krolik, J. H. 2019, MNRAS, 487, 4083, doi: [10.1093/mnras/stz1567](https://doi.org/10.1093/mnras/stz1567)
- Zhang, B.-B., van Eerten, H., Burrows, D. N., et al. 2015, ApJ, 806, 15, doi: [10.1088/0004-637X/806/1/15](https://doi.org/10.1088/0004-637X/806/1/15)
- Zhuang, J., & Shen, R.-F. 2021, Journal of High Energy Astrophysics, 32, 11, doi: [10.1016/j.jheap.2021.06.001](https://doi.org/10.1016/j.jheap.2021.06.001)